RESEARCH ARTICLE

NANO · MICRO small
www.small-journal.com

Redox-Induced Atomic Switch as Platform for Molecular Electronics Devices

Akira Aiba, Marius Buerkle, Satoshi Kaneko,* Tohru Tsuruoka,* Sekito Nishimuro, Kazuya Terabe, and Tomoaki Nishino**

Molecular electronics is attracting increasing attention due to its potential application in post-silicon electronics. However, fabrication of molecular junctions, the fundamental building block of molecular electronic devices, requires complicated procedures, which hamper the efficient development of novel devices. Here, a simple fabrication process by utilizing an atomic switch operated by redox reaction and migration of metal atoms are proposed. The Ta_2O_5-based silver atomic switches are operated with a small operation voltage (0.3 V) in an acetylene atmosphere under an ultra-high vacuum. The consecutive operation of the atomic switch shows novel conductive states around 0.1 G_0 ($G_0 = 2e^2/h$). Inelastic electron tunneling spectra and first-principles calculations reveal that the observed conductive states are attributed to the acetylene molecular junctions on the silver filament. The proposed method accelerates the development of devices through the marriage of molecular junctions with atomic conductive filaments.

1. Introduction

Molecular electronics has been an active research area over the last few decades,[1–5] and molecular junctions are regarded as a promising building block to create the molecular devices as extremely small post-silicon devices.[6–8] Extensive studies were devoted to the development of molecular junctions with a variety of electric functions, e.g., rectifiers,[9,10] switches,[1,11–13] and memories.[14,15] A wealth of knowledge is gained in terms of the creation of the molecular junctions as electric components. The next challenge in molecular electronics is therefore to assemble these components to make a functional device. The obstacle in achieving this goal lies in the formation and operation process of the molecular junctions. Presently, mainly break-junction (BJ) techniques are employed to reliably prepare and activate the molecular junctions.[2–5] The BJ method involves the deformation of the metal electrodes in the junction and consequently necessitates a macroscopic mechanical component, i.e., the electrodes themselves and a piezoelectric device. The macroscopic elements crucially prohibit parallelization and integration of molecular junctions to realize molecular devices with sophisticated functionalities. To overcome these limitations, the use of an atomic switch (AS)[16–20] offers unique opportunities. The AS relies on the formation of a metal atomic filament by ion migration and redox reactions in solid electrolytes such as oxides,[21,22] organic polymers[23,24] or chalcogenides.[17,19] The atomic filament can be reversibly formed and broken down solely by externally applied voltages. The atomic filaments of the AS devices can serve as atomic scale electrodes actuated without mechanical modulations for the molecular junctions. Furthermore, it has been demonstrated

A. Aiba, S. Kaneko, S. Nishimuro, T. Nishino
Department of Chemistry, School of Science
Institute of Science Tokyo
2-12-1 Ookayama, Meguro-ku, Tokyo 152–8550, Japan
E-mail: kaneko.s@mct.isct.ac.jp; tnishino@chem.titech.ac.jp

M. Buerkle
CD-FMat
National Institute of Advanced Industrial Science and Technology (AIST)
Central 2, Umezono 1-1-1, Tsukuba, Ibaraki 305–8568, Japan
E-mail: marius.buerkle@aist.go.jp

The ORCID identification number(s) for the author(s) of this article can be found under https://doi.org/10.1002/smll.202507653

DOI: 10.1002/smll.202507653

T. Tsuruoka, K. Terabe
Research Center for Materials Nanoarchitectonics (MANA)
National Institute for Materials Science (NIMS)
1-1, Namiki, Tsukuba, Ibaraki 305-0044, Japan
E-mail: TSURUOKA.Tohru@nims.go.jp

A. Aiba
Department of Chemical Science and Engineering, School of Materials and Chemical Technology
Institute of Science Tokyo
2-12-1 Ookayama, Meguro-ku, Tokyo 152–8550, Japan

S. Kaneko, S. Nishimuro
Department of Materials Science and Engineering, School of Materials and Chemical Technology
Institute of Science Tokyo
2-12-1 Ookayama, Meguro-ku, Tokyo 152–8550, Japan

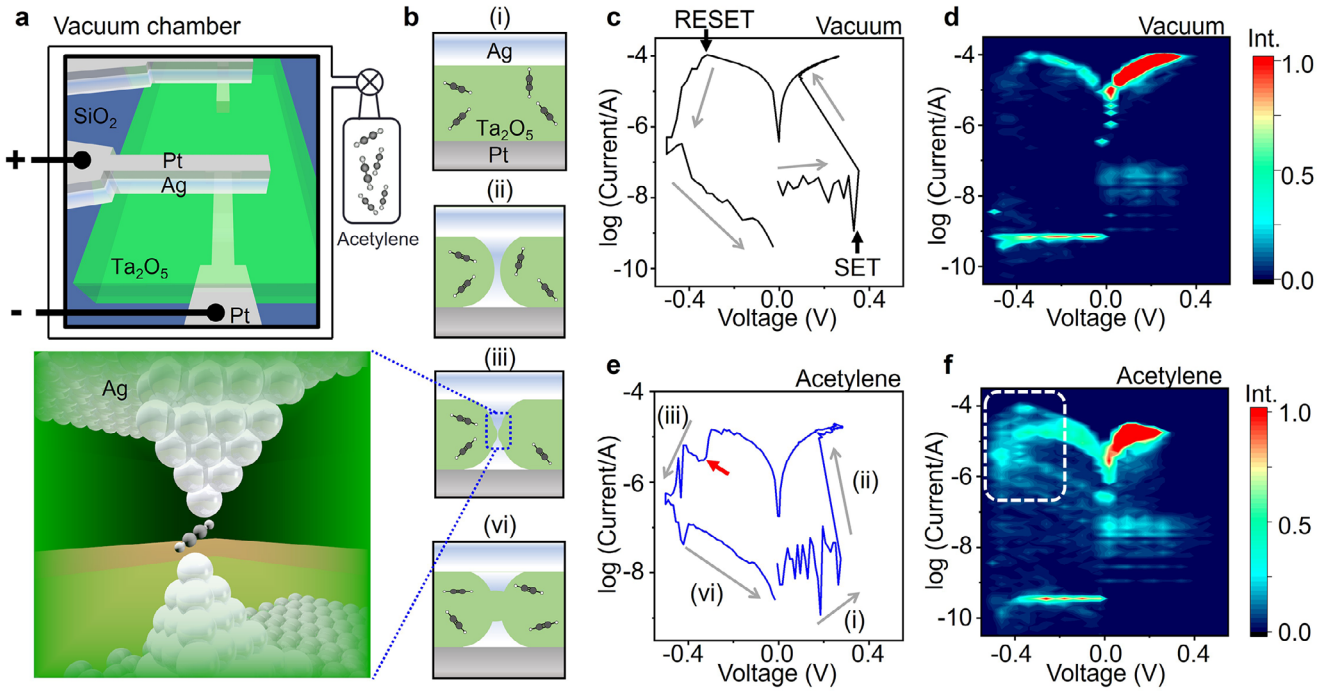

Figure 1. a) Schematic images of the experimental setup for controlling the filament structure with an atomic switch. A sample tube filled with acetylene is connected to the vacuum chamber. b) Schematic illustrations of the formation of the acetylene molecular junction with the atomic switch. First, acetylene molecules percolated into the Ta_2O_5 layer (i). Second, a metal filament formed in the Ta_2O_5 layer when the bias voltage was swept toward the positive direction (SET process) (ii), and then the bias voltage was swept toward the negative direction (RESET process). The acetylene is trapped between the filament residue immediately after the filament rupture, forming the molecular junction (iii). Finally, the molecular junction is ruptured (iv). c, e) *I–V* curves measured in the vacuum (c) and acetylene (e) atmosphere. In the SET process, the formation of the filament decreases the resistance of the sample. Therefore, the effective voltage decreases at the same time as the current increases. d, f) 2D histograms of *I–V* curves measured in vacuum (d) and acetylene (f) atmosphere. The intensity (Int.) was normalized by the maximum histogram count. The numbers of traces used to compile the histograms are 78 (a) and 130 (b).

that the architecture of the AS devices is well suited for massively parallel operations.[16,25] This inherent integrability of the AS devices offers a promising way to integrate the junction to build up molecular computing architecture. Moreover, the coordinated amalgamation of molecular junction function[4,14] and AS device neuromorphic behavior[26,27] holds the promise for the widespread implementation of neuromorphic devices. These advantages render the AS device an ideal platform to improve the formation process of molecular junctions.

In this study, we demonstrate for the first time the successful fabrication of molecular junctions based on AS devices. The AS was operated to form and rupture Ag filaments in its insulating layer containing acetylene, which offers a promising way to wire the molecular electronics.[28] The current-voltage (*I–V*) response demonstrated the emergence of conducting states dominated by the acetylene junction. The conductance states were investigated by supplementary analytical techniques, namely conventional statistical conductance analysis and inelastic electron tunneling spectroscopy (IETS), with a comparison to the simulation by density functional theory (DFT).[29–32] The measured conductance value agree well with the structure model assuming the acetylene single-molecule junction. In IETS, electron–vibration interactions induce abrupt changes in the conductance and allow the detection of vibrational modes as a peak or dip in the derivative of differential conductance, which is caused by the forward and backward scattering of the electron. The IETS corroborated by the DFT calculations characterizes the acetylene trapped between Ag filaments, revealing the immobilization of the acetylene in the Ta_2O_5 layer.

2. Results and Discussion

We fabricated an acetylene molecular junction by the atomic switch break junction (AS-BJ) method, which is implemented for the fabrication of the molecular junction for the first time to the best of our knowledge. The AS-BJ was performed with $Ag/Ta_2O_5/Pt$ gapless-type AS operated in a custom-made vacuum chamber (**Figure 1**a,b, Method, and Sections S1 and S2, Supporting Information). Before examining the formation of the molecular junction, fundamental properties of AS operation were confirmed by *I–V* measurements (Figure 1c). As the bias voltage was swept in the positive direction from 0 V, the current suddenly increased to approximately 0.3 V. This behavior corresponds to the transition of the AS device from the high-resistance (OFF) state to a low-resistance (ON) state and arose from the formation of a Ag filament, referred to as SET process. The subsequent voltage sweep in the negative direction caused the current decrease at approximately −0.3 V by the rupture of the filament (RESET process). The switching performance as shown in Figure 1c agrees with literature.[16,33,34] The point contact

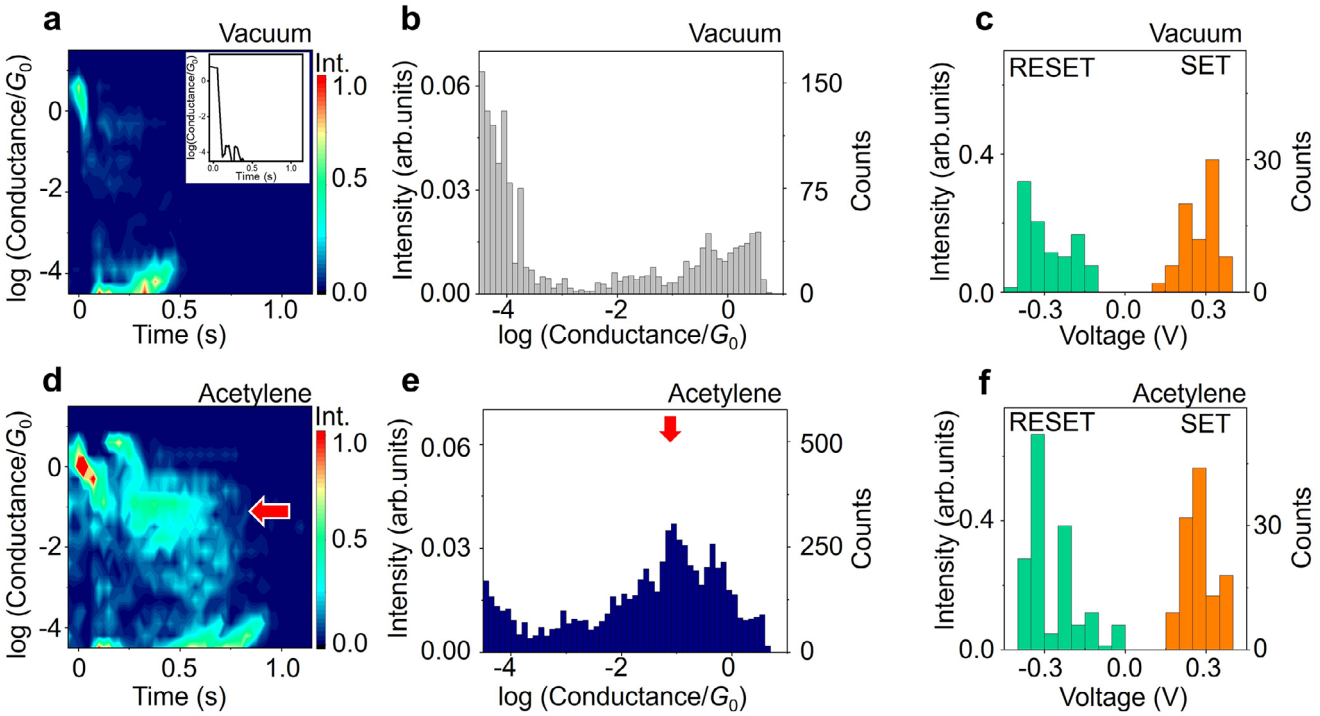

Figure 2. a, d) 2D histograms of conductance traces of the Ag/Ta_2O_5/Pt atomic switch after V_{RESET} was applied in vacuum (a) and in acetylene atmosphere (d). The inset is the typical extracted trace of the RESET process. We set the point at 0.7 G_0 as the origin for the disconnection of the filament and displayed the time course of conductance. The intensity is normalized by the largest counts. The bin size was 0.025 s×0.1 G_0. The numbers of traces are 78 (a) and 130 (b). b,e) Conductance histograms of the Ag/Ta_2O_5/Pt atomic switch in vacuum (b) and acetylene atmosphere e). The numbers of traces are 2465 (b) and 8229 (e). c, f) Distribution of V_{SET} and V_{RESET} under each condition corresponding to (a) and (b).

spectroscopy also support the formation of the Ag filament (Section S3, Supporting Information). Similar measurements were performed in the presence of acetylene (Figure 1e). The Ta_2O_5 layer is considered to absorb acetylene (Section S4, Supporting Information). The *I*–*V* response exhibited a plateau indicated by the red arrow in Figure 1e, where the current stayed nearly constant despite the voltage sweep, during the RESET process, i.e., the rupture of the Ag filament. The constant current signature during the breakdown of atomically thin metal wires has been commonly observed in conventional BJ studies[3–5] and is indicative of the formation of a molecular junction. Thus, Figure 1e suggests the accommodation of an acetylene molecule in the broken Ag filaments. A possible scenario for the formation of an acetylene molecular junction during the operation of the AS is shown in Figure 1b: (i) percolation of acetylene molecules into the Ta_2O_5 layer, (ii) formation of the Ag filament during the SET process,[18,35–37] (iii) formation of the acetylene molecular junction immediately after the rupture of the metal filament during the RESET process, and (iv) breakdown of the molecular junction.

The *I*–*V* responses were statistically evaluated by two-dimensional (2D) histograms constructed by overlaying the *I*–*V* curves (Figure 1d,f). A prominent conducting distribution appeared at the RESET process due to the current plateaus present only in the histogram taken under the acetylene atmosphere (the dashed rectangle in Figure 1f). For the detailed analyses of the conducting states associated with the acetylene molecule, we assessed time evolution of the conductance after applying the voltage to induce the RESET process. The 2D map shows the pronounced conducting states at 10^{-1} G_0 (G_0 stands for the conductance quantum and equals to $2e2/h$, where e and h denote the elementary charge and the Planck constant, respectively) with a lifetime of approximately 0.3 s in the measurements under the acetylene atmosphere (**Figure 2d**), while no noticeable states were found in the absence of acetylene (Figure 2a,b). The distribution of conductance further investigating by 1D conductance histogram in Figure 2e demonstrates that the conductance of the acetylene-induced states is in the order of 10^{-3}-10^{-1} G_0, considering that the conductance of the atomic contact formed in the Ag filament is equal to or larger than 1 G_0.[38] It is noticeable that some traces show the plateau with the integer multiple of 0.2 G_0, indicating the multiple molecules trapped in the nanogap (Section S2, Supporting Information). Besides, the voltages required to activate the SET and RESET processes (V_{SET} and V_{RESET}, respectively) were examined as summarized in the histograms in Figure 2c and f for the absence and presence of acetylene, respectively. The V_{SET} and V_{RESET} values were 0.28 V and -0.28 V in the vacuum and 0.30 V and −0.27 V in the acetylene atmosphere, respectively. Similar operating voltages in both atmospheres indicate that the formation and rupture of the Ag filament are not affected by the presence of acetylene.[22]

To prove the accommodation of the acetylene molecule in the broken Ag filament, we performed IETS measurements. The spectra were acquired by sweeping the DC bias voltage from -400 to +400 mV at 20 K after the AS-BJ reached a stable conducting state (approximately 10^{-3} G_0). Due to AS requiring a

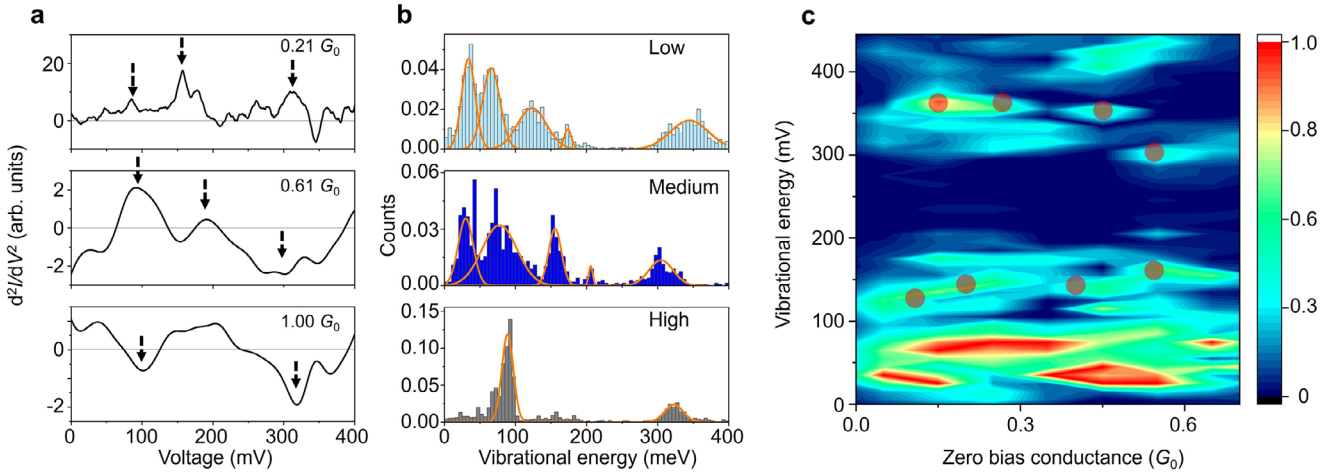

Figure 3. a) Typical d^2I/dV^2 spectra of the acetylene-absorbed atomic switch measured at three different states with different conductance values at $V = 0$. The conductance values were 0.21 G_0 (upper), 0.61 G_0 (middle), and 0.97 G_0 (lower). The peaks (or dips) are defined as the signal with the positive (or negative) intensity of the automatically fitted Gauss function, as shown by the arrows. b) Vibration energy histograms of the acetylene adsorbed atomic switch with different conductance values. The intensity represent the histogram counts normalized by the number of the measured spectra. c) 2D histogram of the conductance and vibrational energy. The intensity of the vibration energy is normalized with respect to the highest intensity of vibration energy below 100 meV. The conductance and energy bin size are 0.1 G_0 and 10 meV, respectively. The gray circle represents the local maximum of the relevant region. The total number of the spectra was 10602. The number of each conductance state is 3467 spectra for the low state, 1472 spectra for the medium, and 1930 spectra for the high state.

higher operation voltage at 20 K (see Section S5, Supporting Information), the atomic configuration of the Ag filament is not affected by the IETS measurements. Utilization of the gradual changes in the junction conductance, which caused by the atomic motion of the Ag filament, allowed us to measure the IETS spectra of the junctions with a range of the conductance: low-conductance region, 0.030 – 0.30 G_0, medium-conductance region, 0.52–0.73 G_0, and high-conductance region, 0.88 – 1.1 G_0 (Section S6, Supporting Information). Since the IETS spectrum could be different even for similar conducting states due to the variation of metal-molecule interactions, we constructed the histogram of the vibrational energy obtained in the IETS spectra in each region to evaluate the vibrational energy. To prepare the histograms, an automated fitting procedure was initially applied to the datasets to extract the peaks present in each IETS spectrum. The peaks (or dips) are defined as the signal with the positive (or negative) intensity of the automatically fitted Gauss function, as shown by the arrows. Subsequently, the vibrational energy histograms were compiled based on the detected peaks. The vibrational energy was determined by the fitting using the Gauss function. The determined vibrational energies were sufficiently distinguished from each other. The histogram counts were normalized by the total number of detected peaks within the specified conductance range (low, medium, and high), thereby facilitating the comparison of histograms across different conductance ranges. **Figure** 3a,b shows typical spectra and histograms of the detected vibrational energy, respectively. The prominent peaks found in Figure 3b were summarized in Section S7 (Supporting Information). The peaks observed in the histogram represent the electron–vibrational interactions induced at the corresponding vibrational energy.[29–32] Vibrational modes with energies less than 100 meV dominated the spectra for the high-conductance states. The low-energy vibrations are ascribed to phonons of Ag and Ta_2O_5 in the AS-BJ devices based on the phonon energies (28 meV for Ag,[37] and 35, 63, and 84 meV for Ta ions[39]). The high-conductance states are, therefore, associated with the Ag filament, being consistent with their conductance values near 1 G_0. In contrast, vibrational modes with energies in the range of 100–400 meV appeared in the spectra for the medium- and low-conductance states. These vibrational modes correspond to the intramolecular vibration of the acetylene molecule,[40] as corroborated by the DFT calculations below. The observation of the acetylene vibrational modes demonstrates the successful formation of the acetylene molecular junctions in the broken Ag filament and that the electron transport in the medium- and low-conductance regimes is governed by the acetylene molecule trapped in the junction. An additional experimental observation is the dependence of the vibrational energies on the conductance of the acetylene molecular junction. Figure 3c shows the 2D mapping of the vibrational energy against the junction conductance for the medium- and low-conductance states, where the vibration modes of the acetylene molecule dominate. It was found that the vibration modes located around 320 meV lowered in energy, while those located around 150 meV became higher energy with an increase of conductance. The behaviors of the vibrational energies originate from electron–vibration interaction altered by the conductance states.[30,31,41]

To elucidate the observed vibrational modes in the junction, we performed DFT calculations for the considered molecular junction. To approximately simulate the BJ experiment, we started from a relaxed structure labeled $\Delta = 0.0$ Å (**Figure** 4a, Section S8, Supporting Information), where the molecule is already captured inside the junction and decrease/increase the electrode separation by 0.4 Å fully relaxing the structure in each step, i.e., assuming an adiabatic junction formation. In the optimized structure, the acetylene molecule connected to the electrode via a C—C bond is perpendicular to the bonding direction, which is reasonable, given the anisotropy of acetylene's π orbitals. Acetylene tends to

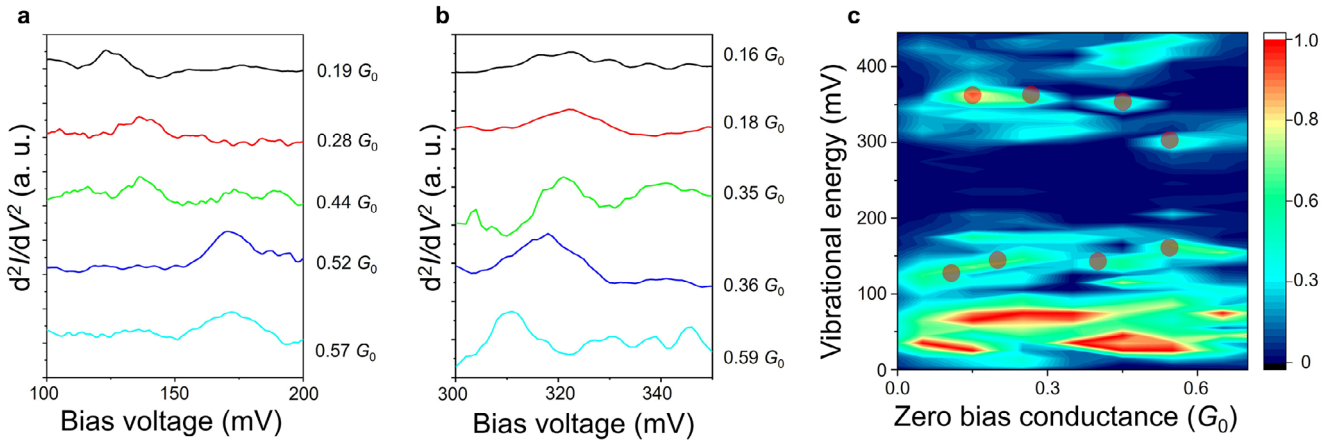

Figure 4. a) Considered pushed/pulled contact geometries. b) Calculated transmission spectra. c) Calculated IET spectra and the observed signals are at energies of the vibrational modes displayed (for example, for Δ = 0.0 Å, the characteristics of the modes remain comparable to that of the other Δ) in the inset.

absorb via the di—σ—π bond on the surface.[42–44] Since the binding energy of acetylene on the Ag surface was estimated to be only 40 meV,[45] the other conformation is thermodynamically unstable. The pushing/pulling steps displayed in Figure 4a are structures where qualitative changes, as compared to the previous step, occur in the IETS. The conductance (transmission at the Fermi energy) changes for these structures decreases from approximately 0.8 G_0 to 10^{-2} G_0 with increasing electrode separation (Figure 4b). When the acetylene forms bonds to the Ag electrodes (Δ0.0 Å), the broad peak attributed to the molecular orbital is observed at 2 eV. The broadened peak attributes to the strong interaction between acetylene and electrodes. Conversely, the peak diminished, and the transmission spectrum exhibited a resemblance to the Ag atomic contact at a distance of 1.6 Å (Figure S9, Supporting Information). To determine the characteristics of the measured vibrational modes (Figure 3a,b), we calculated the corresponding IET spectra (Figure 4c). The two low-energy modes at 71 meV (symmetric bend) and 203 meV (symmetric CC stretching) fit well with the experimentally observed signals at 78 meV and 206 meV, respectively. The higher energy mode at 394 meV (antisymmetric CH stretching), 398 meV (symmetric CH stretching) overestimates the experimentally observed signal 345 meV. The difference between the simulated and experimental values can be attributed to the vibrational anharmonicity and/or the electrode-acetylene interaction at the atomic protrusion.[46,47] The anharmonicity is known to overestimate the vibrational energy, the magnitude of which depends on the vibrational modes.[46] The interaction between the metal electrode surface and the molecule also influences the vibrational energy.[47,48] The atomic protrusions on the electrode that account for these interaction cannot be accurately incorporated in the theoretical model, leading to the deviation of the theoretical prediction from the experimental observations. Therefore, the disorder of the surface structure at the relevant junction might affect vibrational energy. The calculated shift in the vibrational energy induced by changing the electrode separation reproduces the experimental observations. When the separation was increased in the simulations, corresponding to the decrease in conductance in the experiments, the vibrational energy of the symmetric bending mode around 100 meV decreased, whereas the antisymmetric CH stretching around 350 meV increased. This tendency agreed well with the previous one channel model.[41,48] The increased (decreased) separation leads to a weakening (strengthening) of the interaction between the molecule and the electrodes, and it is a well-established fact that the longitudinal vibrational mode energy decreases with decreasing metal-molecule interaction in IETS of H_2 and CO_2 junctions.[41,48] Thus, also in the present study, the decrease in the vibrational energy of the longitudinal modes is attributed to weakened molecule-metal interaction. On the other hand, the vibrational energy of the transversal modes increases due to the enhanced restoring force.[41,48]

The vibrational assignment allows for the interpretation of the systematic change in vibrational energy depending on conductance. As observed in Figure 3c, the vibrational energy of the 100–200 meV (300-400 meV) vibrational mode exhibited an increase (decrease) with increasing conductance. The changes in vibrational energies arise from the alteration of symmetry in the vibrational mode with respect to the direction of the transported electron.[41,48] It is a well-established fact that the longitudinal vibrational mode energy decreases with decreasing metal-molecule interaction in IETS of H_2 and CO_2 junctions. In contrast, the vibrational energy of the transverse vibrational mode increases with the reduction of metal-molecule interaction.[41] In the present case, based on the atomic configuration of the acetylene junction shown in Figure 4, it can be suggested that the π-orbital is orthogonal to the direction of electron transmission. The vibrational modes observed between 200 meV and 400 meV are orthogonal to the π-orbital of acetylene. The CC vibrational mode observed between 100 meV and 200 meV also contains vibrational modes that are mainly parallel to the electron transmission direction, although their contribution to the vertical transmission is still effective.

We discuss the presence of peaks or dips in the IETS that derive from the acetylene vibrational modes. As previously mentioned, the peaks and dips in the conductance represent enhancements and reductions resulting from forward and backward scattering caused by interaction between the electrons and vibrations.

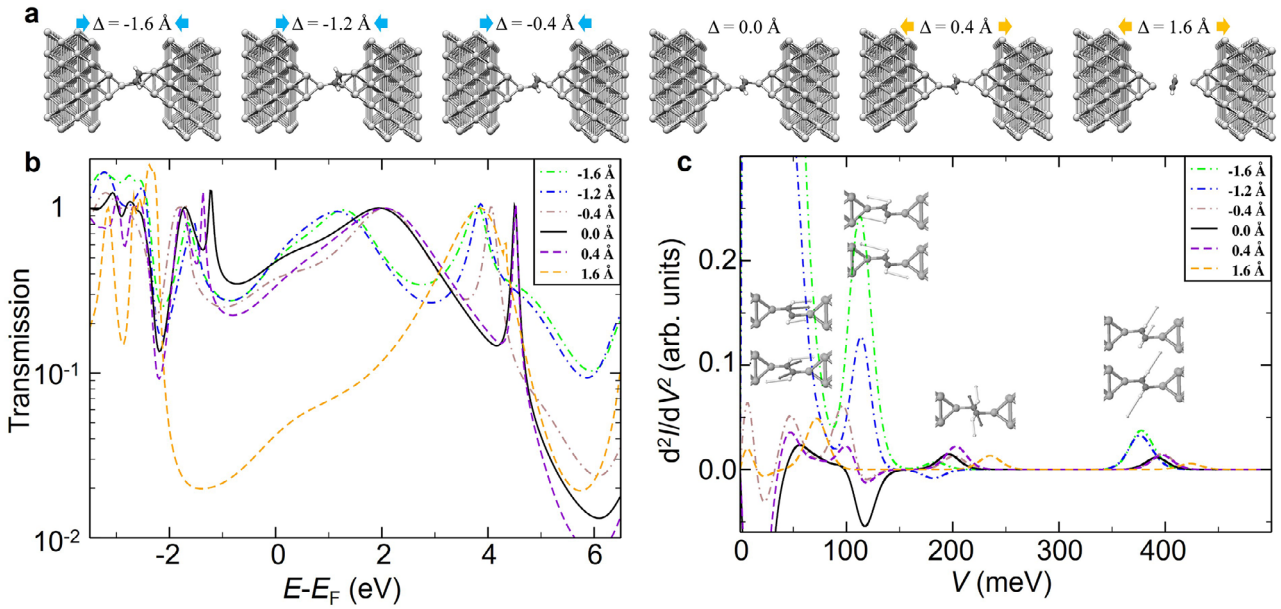

Figure 5. a) vibrational mode observed in 90 meV–200 meV. b) vibrational mode observed in 200 meV–400 meV.

Figure 5 shows the peak/dip histogram of the vibrational modes at 90–200 meV and 200–400 meV. In the 90 to 200 meV region, the electron–vibration scattering is mainly induced by the CC stretching mode, while from 200 to 400 meV, it is mainly induced by symmetric or antisymmetric CH vibrational modes. For the CC stretching mode, the peaks were more frequently observed in the entire conductance region, even above 0.5 G_0, while for the CH vibrational mode, the contribution of the dip increased. Peaks were observed in both vibrational energy regions. In a single-channel model, it is expected that the conductance will enhance due to electron–vibration coupling for the longitudinal vibrational mode, leading to a peak in the d^2I/dV^2 spectra. However, there are exceptions to the matching of the symmetry of the vibrational mode and multichannel contributions.[31,41,49] The orientational change of acetylene or the gap-size modulation gives rise to a variety of conductance states,[30,50] inducing changes in the electron–vibration interaction. The preceding discussion provides sufficient evidence to support the idea that the observed spectrum is derived from the vibrational mode of acetylene and the existence of the acetylene molecule in the low and medium conductance states. Though the Ag-hydrocarbon interaction is relatively small and molecular junction is difficult to fabricate using Ag electrodes,[45,51] our method enables the formation of the acetylene molecular junction with the wide conductance range. The Ta_2O_5 layer facilitates the formation of a molecule that exhibits high conductivity but is thermodynamically unstable. The π conjugated molecule, which has a state near the Fermi energy, can be connected more stably without anchoring groups, improving the conductivity of the molecular junctions.

3. Conclusion

We demonstrated the use of ultrathin metal filaments of atomic switches as electrodes for the formation of acetylene molecular junctions. The repeated SET and RESET processes conducted in an acetylene atmosphere led to the formation of stable conducting states at 10^{-1} G_0. The IETS revealed the vibrational mode associated with the acetylene molecule to demonstrate the formation of the Ag/acetylene/Ag junction, which was rationalized by DFT calculations. The present technique eliminates the need for any mechanical displacements of the metal electrodes in forming molecular junctions. This advantage significantly simplifies the design of molecular devices and, in turn, leads to the parallelization and integration of these devices.

4. Experimental Section

Device Fabrication: Ag/Ta_2O_5/Pt atomic switches were fabricated on a SiO_2-coated Si substrate according to literature.[22,26,52] First, 5-nm-thick Ti and 30-nm-thick Pt layers were formed as the adhesion layer and the bottom electrode, respectively, by electron beam (EB) deposition. Next, a Ta_2O_5 layer as the ion-conducting electrolyte was deposited by radio-frequency sputtering using a polycrystalline target with a 77% Ar and 23% O_2 gas mixture (Section S2, Supporting Information). Finally, 30-nm-thick Ag and Pt layers were deposited as the top electrode and the coat layer, respectively, by EB deposition. Each atomic switch on the substrate had a cross-wire structure with a junction area of 5 μm × 5 μm.

Electrical Measurements: The *I–V* measurements were performed in a vacuum chamber (Vacuum & Optical Instruments, Tokyo, Japan) at a base pressure of 10^{-3} Pa. The acetylene molecule was introduced at 200 Pa to the chamber via capillary. IETS measurements were carried out at the liquid helium temperature for the atomic switch with the conducting states at approximately 10^{-1} G_0. The details of the electrical circuit for the *I–V* and IETS measurements can be found in the Section S1 (Supporting Information).

Supporting Information

Supporting Information is available from the Wiley Online Library or from the author.

Acknowledgements

This work was partially supported by a Grant-in-Aid for Scientific Research (20K05445, 22H04974), JSPS A3 Foresight Program from MEXT, research granted from Murata Science and Education Foundation, the Tokyo Institute of Technology Research fund (Challenging Research Award).

Conflict of Interest

The authors declare no conflict of interest.

Data Availability Statement

The data that support the findings of this study are available from the corresponding authors on request.

Keywords

acetylene, atomic switch, conductive filament, inelastic electron tunneling spectroscopy, molecular electronic device, single-molecule junction

Received: June 25, 2025
Revised: September 22, 2025
Published online: October 25, 2025

[1] X. Xu, C. Gao, R. Emusani, C. Jia, D. Xiang, *Adv. Sci.* **2024**, *11*, 2400877.
[2] X. Xie, P. Li, Y. Xu, L. Zhou, Y. Yan, L. Xie, C. Jia, X. Guo, *ACS Nano* **2022**, *16*, 3476.
[3] F. Evers, R. Korytár, S. Tewari, J. M. van Ruitenbeek, *Rev. Mod. Phys.* **2020**, *92*, 035001.
[4] N. Xin, J. Guan, C. Zhou, X. Chen, C. Gu, Y. Li, M. A. Ratner, A. Nitzan, J. F. Stoddart, X. Guo, *Nat. Rev. Phys.* **2019**, *1*, 211.
[5] T. A. Su, M. Neupane, M. L. Steigerwald, L. Venkataraman, C. Nuckolls, *Nat. Rev. Mater.* **2016**, *1*, 16002.
[6] R. Hanson, L. P. Kouwenhoven, J. R. Petta, S. Tarucha, L. M. K. Vandersypen, *Rev. Mod. Phys.* **2007**, *79*, 1217.
[7] C. Joachim, J. K. Gimzewski, A. Aviram, *Nature* **2000**, *408*, 541.
[8] B. K. Teo, X. H. Sun, *Chem. Rev.* **2007**, *107*, 1454.
[9] I. Díez-Pérez, J. Hihath, Y. Lee, L. Yu, L. Adamska, M. A. Kozhushner, I. I. Oleynik, N. Tao, *Nat. Chem.* **2009**, *1*, 635.
[10] A. C. Aragonès, N. Darwish, S. Ciampi, F. Sanz, J. J. Gooding, I. Diez-Perez, *Nat. Commun.* **2017**, *8*, 15056.
[11] D. Dulić, S. J. van der Molen, T. Kudernac, H. T. Jonkman, J. J. de Jong, T. N. Bowden, J. van Esch, B. L. Feringa, B. J. van Wees, *Phys. Rev. Lett.* **2003**, *91*, 207402.
[12] L. Venkataraman, J. E. Klare, C. Nuckolls, M. S. Hybertsen, M. L. Steigerwald, *Nature* **2006**, *442*, 904.
[13] Y. Li, M. Buerkle, G. Li, A. Rostamian, H. Wang, Z. Wang, D. R. Bowler, T. Miyazaki, L. Xiang, Y. Asai, G. Zhou, N. Tao, *Nat. Mater.* **2019**, *18*, 357.
[14] H. Jeong, D. Kim, D. Xiang, T. Lee, *ACS Nano* **2017**, *11*, 6511.
[15] M. Min, S. Seo, S. M. Lee, H. Lee, *Adv. Mater.* **2013**, *25*, 7045.
[16] T. Hasegawa, K. Terabe, T. Tsuruoka, M. Aono, *Adv. Mater.* **2012**, *24*, 252.
[17] K. Terabe, T. Hasegawa, T. Nakayama, M. Aono, *Nature* **2005**, *433*, 47.
[18] T. Tsuruoka, T. Hasegawa, K. Terabe, M. Aono, *J. Electroceram* **2017**, *39*, 143.
[19] J. Kim, J. Lee, M. Kang, H. Sohn, *Nanoscale Res. Lett.* **2021**, *16*, 128.
[20] K. S. Scharnhorst, J. P. Carbajal, R. C. Aguilera, E. J. Sandouk, M. Aono, A. Z. Stieg, J. K. Gimzewski, *Jpn. J. Appl. Phys.* **2018**, *57*, 03ED02.
[21] C. Arima, A. Suzuki, A. Kassai, T. Tsuruoka, T. Hasegawa, *J. Appl. Phys.* **2018**, *124*, 152114.
[22] A. Aiba, S. Kaneko, T. Tsuruoka, K. Terabe, M. Kiguchi, T. Nishino, *Appl. Phys. Lett.* **2020**, *117*, 233104.
[23] K. Krishnan, M. Aono, T. Tsuruoka, *Nanoscale* **2016**, *8*, 13976.
[24] B. Cho, J. M. Yun, S. Song, Y. Ji, D. Y. Kim, T. Lee, *Adv. Funct. Mater.* **2011**, *21*, 3976.
[25] J. J. Yang, D. B. Strukov, D. R. Stewart, *Nat. Nanotechnol.* **2013**, *8*, 13.
[26] T. Tsuruoka, T. Hasegawa, K. Terabe, M. Aono, *Mater. Res. Soc. Symp. Proc.* **2013**, *1562*, 8.
[27] Z. Wang, S. Joshi, S. E. Savel'ev, H. Jiang, R. Midya, P. Lin, M. Hu, N. Ge, J. P. Strachan, Z. Li, Q. Wu, M. Barnell, G. L. Li, H. L. Xin, R. S. Williams, Q. Xia, J. J. Yang, *Nat. Mater.* **2017**, *16*, 101.
[28] Y. Okawa, M. Aono, *Nature* **2001**, *409*, 683.
[29] B. C. Stipe, M. A. Rezaei, W. Ho, *Science* **1998**, *280*, 1732.
[30] R. Smit, Y. Noat, C. Untiedt, N. Lang, M. v. van Hemert, J. Van Ruitenbeek, *Nature* **2002**, *419*, 906.
[31] O. Tal, M. Krieger, B. Leerink, J. M. van Ruitenbeek, *Phys. Rev. Lett.* **2008**, *100*, 196804.
[32] R. Fukuzumi, M. Buerkle, Y. Li, S. Kaneko, P. Li, S. Kobayashi, S. Fujii, M. Kiguchi, H. Nakamura, K. Tsukagoshi, T. Nishino, *Small* **2021**, *17*, 2008109.
[33] J. J. T. Wagenaar, M. Morales-Masis, J. M. van Ruitenbeek, *J. Appl. Phys.* **2012**, *111*, 014302.
[34] A. Nayak, T. Tamura, T. Tsuruoka, K. Terabe, S. Hosaka, T. Hasegawa, M. Aono, *J. Phys. Chem. Lett.* **2010**, *1*, 604.
[35] I. Valov, I. Sapezanskaia, A. Nayak, T. Tsuruoka, T. Bredow, T. Hasegawa, G. Staikov, M. Aono, R. Waser, *Nat. Mater.* **2012**, *11*, 530.
[36] M. Lübben, S. Menzel, S. G. Park, M. Yang, R. Waser, I. Valov, *Nanotechnology* **2017**, *28*, 135205.
[37] A. Aiba, R. Koizumi, T. Tsuruoka, K. Terabe, K. Tsukagoshi, S. Kaneko, S. Fujii, T. Nishino, M. Kiguchi, *ACS Appl. Mater. Interfaces* **2019**, *11*, 27178.
[38] N. Agraït, A. L. Yeyati, J. M. Van Ruitenbeek, *Phys. Rep.* **2003**, *377*, 81.
[39] H. Ono, Y. Hosokawa, K. Shinoda, K. Koyanagi, H. Yamaguchi, *Thin Solid Films* **2001**, *381*, 57.
[40] S. Hengrasmee, J. B. Peel, *Surf. Sci.* **1987**, *184*, 434.
[41] R. Ben-Zvi, R. Vardimon, T. Yelin, O. Tal, *ACS Nano* **2013**, *7*, 11147.
[42] C. Jimenez-Orozco, E. Florez, A. Moreno, P. Liu, J. A. Rodriguez, *Phys. Chem. Chem. Phys.* **2017**, *19*, 1571.
[43] H. Ibach, S. Lehwald, *J. Vac. Sci. Technol.* **1978**, *15*, 407.
[44] F. Mittendorfer, C. Thomazeau, P. Raybaud, H. Toulhoat, *J. Phys. Chem. B* **2003**, *107*, 12287.
[45] Y. Huang, H. L. Lu, Z. X. Chen, *Phys. Chem. Chem. Phys.* **2022**, *24*, 3182.
[46] T. Joutsuka, K. Ando, *J. Chem. Phys.* **2011**, *134*, 204511.
[47] I. Rahinov, A. Kandratsenka, T. Schafer, P. Shirhatti, K. Golibrzuch, A. M. Wodtke, *Phys. Chem. Chem. Phys.* **2024**, *26*, 15090.
[48] D. Djukic, K. S. Thygesen, C. Untiedt, R. H. M. Smit, K. W. Jacobsen, J. M. van Ruitenbeek, *Phys. Rev. B* **2005**, *71*, 161402(R).
[49] M. Galperin, M. A. Ratner, A. Nitzan, *J. Chem. Phys.* **2004**, *121*, 11965.
[50] S. Kobayashi, S. Kaneko, M. Kiguchi, K. Tsukagoshi, T. Nishino, *J. Phys. Chem. Lett.* **2020**, *11*, 6712.
[51] R. Fukuzumi, S. Kaneko, S. Fujii, T. Nishino, M. Kiguchi, *ChemPhysChem* **2020**, *21*, 175.
[52] T. Tsuruoka, I. Valov, S. Tappertzhofen, J. van den Hurk, T. Hasegawa, R. Waser, M. Aono, *Adv. Funct. Mater.* **2015**, *25*, 6374.